Available online at www.sciencedirect.com
SCIENCE DIRECT®
Journal of volcanology and geothermal research
ELSEVIER
Journal of Volcanology and Geothermal Research 122 (2003) 281–294
www.elsevier.com/locate/jvolgeores

# Mechanisms for ground-surface fracturing and incipient slope failure associated with the 2001 eruption of Mt. Etna, Italy: analysis of ephemeral field data

Andrea Billi [a,*], Valerio Acocella [a], Renato Funiciello [a], Guido Giordano [a], Gianni Lanzafame [b], Marco Neri [b]

[a] *Dipartimento di Scienze Geologiche, Università 'Roma Tre', Largo S.L. Murialdo 1, 00146 Rome, Italy*
[b] *Istituto Nazionale di Geofisica e Vulcanologia, Piazza Roma 2, 95123 Catania, Italy*

Received 16 April 2002; accepted 27 November 2002

**Abstract**

During the July–August 2001 eruption of Mt. Etna development of extensional fractures/faults and grabens accompanied magma intrusion and subsequent volcanic activity. During the first days of the eruption, we performed an analysis of attitude, displacement and propagation of fractures and faults exposed on the ground surface in two sites, Torre del Filosofo and Valle del Leone, located along the same fracture system in the region surrounding the Valle del Bove depression on the eastern flank of Mt. Etna. Fractures and faults formed as the consequence of a shallow intruding dyke system that fed the several volcanic centres developed along the fracture system. The investigated sites differ in slope attitude and in geometrical relationships between fractures and slopes. In particular, the fracture system propagated parallel to the gentle slope ($<7°$ dip) in the Torre del Filosofo area, and perpendicular to the steep slope ($\sim 25°$ dip) in the Valle del Leone area. In the Torre del Filosofo area, slight graben subsidence and horizontal extension of the ground surface by about 3 m were recorded. In the Valle del Leone area, extensional faulting forming a larger and deeper graben with horizontal extension of the ground surface by about 10 m was recorded. For the Valle del Leone area, we assessed a downhill dip of 14° for the graben master fault at the structural level beneath the graben where the fault dip shallows. These results suggest that dyke intrusion at Mount Etna, and particularly in the region surrounding the Valle del Bove depression, may be at the origin of slope failure and subsequent slumps where boundary conditions, i.e. geometry of dyke, slope dip and initial shear stress, amongst others, favour incipient failures.


*Keywords:* Mount Etna; dykes; extensional fractures; grabens; slope failures

## 1. Introduction

Since the giant collapse of the Mt. St. Helens volcano, which occurred at the onset of the May 1980 eruption (Voight et al., 1983; Sparks et al., 1986), flank collapses of volcanoes have been recognised as major processes in their development and evolution (e.g. Ellis and King, 1991; Holcomb and Searle, 1991; Masson et al., 2002),

* Corresponding author. Fax: +39-6-54888201.
*E-mail address:* billi@uniroma3.it (A. Billi).

0377-0273/03/$ – see front matter © 2003 Elsevier Science B.V. All rights reserved.
doi:10.1016/S0377-0273(02)00507-3

and as significant sources of hazard (e.g. Siebert et al., 1987; Elsworth et al., 1999; Reid et al., 2001). Potential flank failures are particularly hazardous in the case of island volcanoes, for the potential of generating tsunamis that may travel hundreds of kilometres (e.g. Moore and Moore, 1984). In view of such a potential hazard, the identification of precursors to flank collapses is now a critical problem addressed by several studies on volcanoes (e.g. van Wyk de Vries and Francis, 1997; Day et al., 1999; Finn et al., 2001). Catastrophic flank failures are likely to occur on steep flanks during eruptions, triggered by a number of processes including magma intrusions (e.g. Siebert, 1984; Elsworth and Day, 1999) such as dyke emplacement. The emplacement of dykes commonly generates extensional faulting and fracturing at the Earth's surface and subsequent graben subsidence (e.g. Bjornsson et al., 1977; Abdallah et al., 1979; Gudmundsson, 1983, 1995; Pollard et al., 1983; Bousquet et al., 1984; Murray and Pullen, 1984; Mastin and Pollard, 1988; Rubin and Pollard, 1988; Morgan, 1991). Dyke emplacement may be at the origin of catastrophic flank collapses, particularly on steep-sided volcanoes (e.g. Elsworth and Day, 1999). Information on ground-surface deformations before, during and after volcanic eruptions is fundamental to evaluate parameters such as the geometry and dimensions of feeder dykes (Fink, 1985; Fink and Pollard, 1983), the depth of magma storage (Wadge, 1977; Dobran and Coniglio, 1996), the displacement in the volcano interior (Dowden et al., 1995, 1997) and, therefore, the potential flank instability (McGuire et al., 1990). Intrusion-related deformations have been investigated before, during, and after volcanic eruptions, by applying different methods, such as direct measurements of displacements across fractures, or geodetic surveys (e.g. Mogi, 1958; Walsh and Decker, 1971; Pollard et al., 1983; Murray and Pullen, 1984; Okamura et al., 1988; Hoffmann et al., 1990; Rubin, 1992; Dowden et al., 1995, 1997; Bonaccorso, 1999). Measurements of the deformation associated with dyke emplacement can be difficult to make as the emplacement of lava flows or pyroclastic flows frequently covers the deformed area shortly after the deformation occurred.

During the July–August 2001 eruption of Mt. Etna (Fig. 1), a more than 6000 m long, N–S to NNE–SSW system of extensional fractures and faults developed on top of Mt. Etna, along the western rim of the Valle del Bove depression (Fig. 2a,b). Most of the fractures were exposed only for a few hours/days on the ground surface and then were covered by lava flows. Extensional displacement and throw occurred on fractures and associated graben subsidence developed (e.g. Parfitt and Peacock, 2001; Peacock and Parfitt, 2002). In the northern sector, the fracture system propagated across the rim of the Valle del Bove depression and caused an incipient slope failure along its steep flank (Valle del Leone in Figs. 1a and 2c).

In this paper, we analyse fracture azimuth, propagation and displacement data collected in two areas across the active fracture system during the July–August 2001 eruption of Mt. Etna: the Valle del Leone and the Torre del Filosofo areas (Fig. 2). The data collected at the Torre del Filosofo area were ephemeral, owing to lava and pyroclastic flows, which covered them 48–72 h after they occurred, and dangerous to be gathered owing to a close (30–250 m) active spatter cone. We used fracture displacement and propagation data collected in the field to understand how extensional fractures, graben subsidence and incipient slope failure might have developed in relation to intrusive activity. Understanding how, why and where volcano slopes can collapse is paramount to evaluate immediate hazard. In this view, our results may be useful in predicting conditions under which future slope failures at Mt. Etna and other volcanoes may occur, and in defining precursors of these failures. Numerical simulations of the mechanisms triggering slope failures may benefit by the field observations discussed hereafter.

## 2. Geological setting

With a height of over 3300 m and an elliptical base with axes 38 and 47 km in length, respectively, Mt. Etna (Fig. 1) is the largest active onshore volcano in Europe. It lies on continental

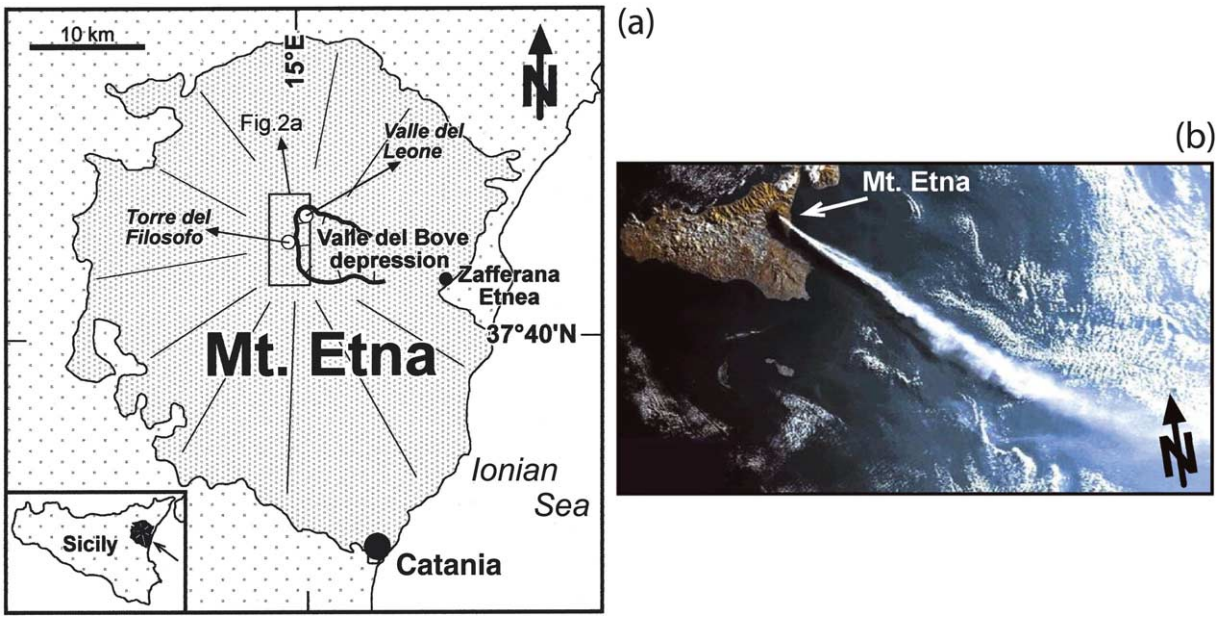


Fig. 1. (a) Location map for Torre del Filosofo and Valle del Leone study areas on top of Mt. Etna volcano. (b) Landsat image of Mt. Etna and Sicily on 21 July 2001. Note the volcano shooting southeastward a plume of ash and gases arcing in the Mediterranean Sea.

crust close to the subduction-related Aeolian magmatic arc, although it shows oceanic basalt affinities and no traces of subducted materials (Barberi et al., 1974; Tanguy et al., 1985; Allard et al., 1991, 1997).

Volcanic activity at Mt. Etna started more than 500 kyr ago by both submarine and subaerial fissural eruptions (Romano, 1982). About 200 kyr ago the activity changed from fissural to central and generated a large strato-volcano. The Ellittico volcano, whose activity started 34 kyr ago, reached more than 3800 m in height. The Ellittico volcano ended its activity about 15 kyr ago with the collapse of a caldera as a consequence of Plinian eruptions. The present Mt. Etna volcano has been growing from the collapsed area during the last 15 kyr (Romano, 1982; Calvari et al., 1992; Coltelli et al., 1994, 1998; Gillot et al., 1994; Garduño et al., 1997). At present, Mt. Etna comprises a series of partially nested volcanoes, characterised by summit calderas (Condomines et al., 1995). Through time, the eruptive axis has progressively shifted westwards.

Earthquake data suggest a spatial variation in the present stress field beneath Mt. Etna, from compressive (west, $>10\,000$ m deep) to both tensile and compressive (east, $<10\,000$ m deep) (Cocina et al., 1997). Extensional and contractional faulting on the eastern flank is well-documented (Lanzafame et al., 1997a,b; Azzaro, 1999).

The Valle del Bove depression (Fig. 1) bisects the volcanic edifice in its eastern sector. The western rim of this depression has been a preferential location for repeated N–S dyke injection (Bousquet and Lanzafame, 2001) and consequent dyke-induced collapses causing a progressive westward migration of the depression rim (McGuire et al., 1990, 1997; Rymer et al., 1993).

## 3. The July–August 2001 eruption

The July–August 2001 eruption of Mt. Etna (Table 1) began on 17 July and lasted 24 days (Stone, 2001). The eruption was heralded by more than 2600 earthquakes with magnitude $>1.7$, which occurred from the night of 12–13 July at progressively shallower depths from 3000 m

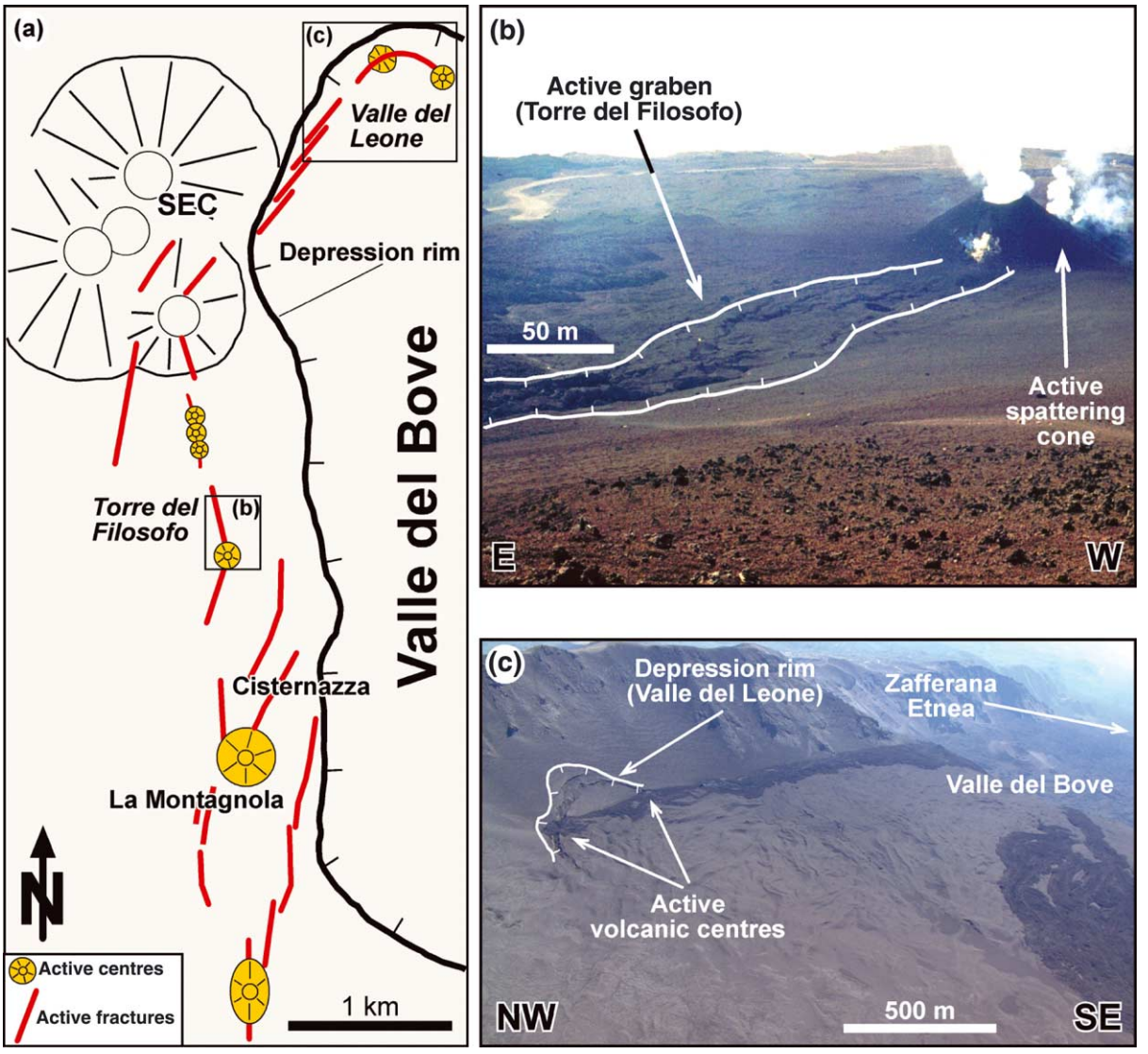


Fig. 2. (a) Schematic map of fractures and volcanic centres developed during the July–August 2001 eruption of Mt. Etna. (b) Photograph of the Torre del Filosofo study area during the eruption (19 July 2001, 15.00 h GMT). Note the line drawing representing the graben rim. (c) Photograph from helicopter of the Valle del Leone study area (21 July 2001, 11.00 h GMT). Note the line drawing representing the rim of the slope failure.

below sea level to more than 1000 m above sea level, with a maximum epicentral concentration corresponding to the La Montagnola area (Fig. 2a) (Patanè et al., 2002).

The night before the onset of the eruption, i.e. the night of 16–17 July, a 1400 m long, 500 m wide and NNE–SSW-trending graben formed in the Cisternazza area (Fig. 2a). The eruption started early in the morning of 17 July with lava fountaining and lava flow from the Southeast Crater (SEC in Fig. 2a). At 05.00 h GMT a NNE-trending eruptive fracture system developed at the base of the Southeast Crater. The same day, at 15.00 h GMT, the eruptive fracture system started to extend southward, i.e. downhill towards the Torre del Filosofo area (Fig. 2a), producing a

Table 1
Major ground-surface deformations and volcanic activity occurred during the July–August 2001 eruption of Mt. Etna

| Day | Time | Location | Ground-surface deformations | Volcanic activity |
|---|---|---|---|---|
| 13–16 July | starting on 13 July early morning | La Montagnola | ground swelling up to 0.2 m | absent |
| 16–17 July | night | Cisternazza | fractures+ NNE graben, 1400 m long, 500 m wide | absent |
| 17 July | starting in the early morning | SEC | eruptive NNE fractures | lava fountaining and effusion |
| 17 July | starting at 05.00 h GMT | south slope of SEC | fractures+ N–S graben, 400 m long, 50 m wide | lava effusion for 16 days |
| 17 July | starting at 15.00 h GMT | Torre del Filosofo | fractures+ NNW graben, 450 m long, 30–50 m wide | effusive for 23 days+ strombolian episodes |
| 18 July | starting at 00.20 h GMT | south of La Montagnola | eruptive NNE fractures | lava spattering for 23 days from along-fracture vents |
| 19 July | starting at 17.00 h GMT | Piano del Lago | collapse of pit craters | phreatomagmatic+ strombolian+ effusive for 18 days |
| 20 July | starting in the afternoon | Valle del Leone | fractures+ arched graben | effusive+ mild eruptive for 10 days |
| 23 July | starting in the morning | southeast slope of SEC | eruptive NNE fractures | effusive for 3 days |

N165°-trending, 450 m long and 30–50 m wide graben. The segmented and complex fracture system grew for about 12 h. Fracture growth in the Torre del Filosofo area terminated during the night of 17–18 July. Several vents and hornitos were active along the fracture system, feeding lava flows. The Torre del Filosofo study area (2700 m above sea level) includes the northern portion of this graben (Fig. 2b). The ground surface in the graben was displaced vertically up to a maximum of 1 m. On 19 July, in the afternoon, we collected a set of fracture azimuth and displacement data across the northern portion of the graben developed in this area (Table 2). The following day, the study area was entirely covered by lava flows.

On 18 July a new fracture set propagated upslope for about 700 m along the S–N direction south of the La Montagnola area. Several eruptive vents occurred along this fracture set and fed a lava flow for 23 days.

On 19 July at 17.00 h GMT a phreatomagmatic activity began from five vents formed along and within the graben occurred in the Cisternazza area. On 25 July the volcanic activity of these vents shifted from phreatomagmatic to strombolian and effusive, and then became phreatomagmatic again after 1 August.

Table 2
List of fracture data collected in the Torre del Filosofo area

| No. | Azimuth | Aperture (m) | Distance from origin (m) | |
|---|---|---|---|---|
| 1 | N350° | 0.030 | 1.11 | A–A′ scan line |
| 2 | N347° | 0.045 | 2.14 | |
| 3 | N343° | 0.030 | 3.06 | |
| 4 | N334° | 0.050 | 5.47 | |
| 5 | N334° | 0.040 | 7.75 | |
| 6 | N339° | 0.710 | 9.92 | |
| 7 | N335° | 0.830 | 12.21 | |
| 8 | N343° | 0.105 | 13.11 | |
| 9 | N335° | 0.030 | 15.74 | |
| 10 | N336° | 0.050 | 18.09 | |
| 11 | N338° | 0.980 | 23.73 | |
| 12 | N343° | 0.50 | 1.0 | B–B′ scan line |
| 13 | N335° | 0.30 | 7.5 | |
| 14 | N348° | 0.30 | 12.0 | |
| 15 | N342° | 0.30 | 15.0 | |
| 16 | N342° | 0.70 | 18.5 | |
| 17 | N330° | 0.40 | 24.5 | |
| 18 | N338° | 0.40 | 26.5 | |
| 19 | N348° | 0.20 | 29.5 | |
| 20 | N352° | 0.30 | 35.5 | |
| 21 | N336° | | | |
| 22 | N350° | | | |
| 23 | N340° | | | |
| 24 | N344° | | | |
| 25 | N344° | | | |
| 26 | N335° | | | |
| 27 | N344° | | | |
| 28 | N351° | | | |
| 29 | N342° | | | |
| 30 | N321° | | | |
| 31 | N333° | | | |
| 32 | N334° | | | |
| 33 | N354° | | | |
| 34 | N322° | | | |
| 35 | N335° | | | |
| 36 | N335° | | | |
| 37 | N339° | | | |
| 38 | N349° | | | |
| 39 | N330° | | | |
| 40 | N329° | | | |
| 41 | N337° | | | |
| 42 | N347° | | | |
| 43 | N342° | | | |
| 44 | N339° | | | |
| 45 | N351° | | | |
| 46 | N343° | | | |

These data were exposed on the volcano ground surface only for about 48–72 h and then were covered by lava flows. Note that data numbers 1–11 refer to the A–A′ scan line (Fig. 3d), and data numbers 12–20 refer to the B–B′ scan line (Fig. 3e).

On 20 July, a NNE-striking fracture set generated to the northeast of the Southeast Crater and formed a family of en échelon fissures about 1800 m long (Fig. 2a). Fractures propagated across the rim of the Valle del Bove depression and, at the northern tip, terminated in the Valle del Leone area (2680 m above sea level). Fractures formed a fault-bounded, arc-shaped graben that paralleled the steep flank of the depression (Fig. 2a). The same day, lava flowed from a vent located in the apex of the arched graben and then from a hornito located at the southeastern tip (Fig. 2c). On 21 July, we surveyed the Valle del Leone area and collected fracture azimuth and displacement data (Table 3).

On 23 July a new eruptive fracture set trending N170° formed on the southeastern slope of the Southeast Crater and fed a small lava flow for 3 days.

Although lava flows kept running up to about 10 August, the initiation and growth of fractures and associated grabens terminated by 24 July (Table 1).

## 4. Data analysis

### 4.1. Torre del Filosofo area

The investigated site includes a roughly flat area (i.e. dipping less than 7° SSE) where the above-mentioned graben and volcanic centres were generated during the eruption (Figs. 2b and 3a). The graben and volcanic centres developed along the SSE-striking fracture system, i.e. parallel to the gentle slope of the Torre del Filosofo area (Fig. 3a). Fractures in this area are high-angle extensional features across which the ground surface is horizontally displaced by up to 1 m (i.e. fracture aperture in Table 2). Fracture azimuths vary between N9°W and N39°W (Fig. 3b). The average fracture azimuth, computed by best fitting the population with a unimodal Gaussian distribution (e.g. Salvini et al., 1999), is N19°W (Fig. 3b). We measured the opening displacement (i.e. aperture) of each fracture along two N70°E-oriented scan lines (A–A′ and B–B′ in Fig. 3a). The average azimuth of fractures in-

Table 3
List of fracture data collected in the Valle del Leone area

| No. | Azimuth | No. | Azimuth |
|---|---|---|---|
| 1 | N267° | 50 | N197° |
| 2 | N253° | 51 | N228° |
| 3 | N255° | 52 | N226° |
| 4 | N238° | 53 | N232° |
| 5 | N249° | 54 | N245° |
| 6 | N241° | 55 | N243° |
| 7 | N243° | 56 | N231° |
| 8 | N248° | 57 | N227° |
| 9 | N244° | 58 | N249° |
| 10 | N242° | 59 | N237° |
| 11 | N249° | 60 | N236° |
| 12 | N269° | 61 | N222° |
| 13 | N263° | 62 | N280° |
| 14 | N258° | 63 | N221° |
| 15 | N247° | 64 | N241° |
| 16 | N249° | 65 | N227° |
| 17 | N253° | 66 | N229° |
| 18 | N240° | 67 | N257° |
| 19 | N241° | 68 | N244° |
| 20 | N237° | 69 | N246° |
| 21 | N241° | 70 | N259° |
| 22 | N240° | 71 | N250° |
| 23 | N246° | 72 | N242° |
| 24 | N242° | 73 | N219° |
| 25 | N243° | 74 | N199° |
| 26 | N249° | 75 | N240° |
| 27 | N258° | 76 | N238° |
| 28 | N251° | 77 | N230° |
| 29 | N253° | 78 | N212° |
| 30 | N268° | 79 | N246° |
| 31 | N243° | 80 | N247° |
| 32 | N252° | 81 | N240° |
| 33 | N257° | 82 | N235° |
| 34 | N251° | 83 | N235° |
| 35 | N268° | 84 | N219° |
| 36 | N240° | 85 | N222° |
| 37 | N244° | 86 | N218° |
| 38 | N251° | 87 | N213° |
| 39 | N224° | 88 | N186° |
| 40 | N235° | 89 | N209° |
| 41 | N233° | 90 | N198° |
| 42 | N230° | 91 | N197° |
| 43 | N255° | 92 | N200° |
| 44 | N249° | 93 | N203° |
| 45 | N233° | 94 | N212° |
| 46 | N255° | 95 | N211° |
| 47 | N226° | 96 | N224° |
| 48 | N223° | 97 | N237° |
| 49 | N222° | 98 | N236° |

cluded in the scan lines is N20°W (Fig. 3c). We plotted the fracture aperture as cumulated value along the scan line against the scan-line distance (Fig. 3d,e). Fig. 3d shows a cumulated extensional displacement of 2.9 m, accommodated over 11 extensional fractures along the A–A′ scan line. In particular, 52% of the extensional displacement is accommodated by three fractures: two in the middle portion of the scan line and one on the eastern side. The vertical displacement of the ground surface on the A–A′ section reaches a maximum value of 0.7 m. Fig. 3e shows a cumulated extensional displacement of 3.4 m accommodated over nine extensional fractures along the B–B′ scan line. This displacement is homogeneously accommodated across the nine fractures as suggested by the roughly linear trend in the diagram (see also Table 3). The vertical displacement of the ground surface on the B–B′ scan line reaches a maximum value of 1 m.

### 4.2. Valle del Leone area

The investigated site is located within the Valle del Bove depression along its northwestern margin (Fig. 2a,c). Fractures in this area are extensional features that grew at the toe of a 24° steep, arc-shaped slope (Fig. 4a). Fractures and faults formed a graben with a semicircular shape, which parallels the rim of the Valle del Bove depression. We measured fracture and fault azimuth and displacement in the central and western portion of the graben (Table 3). Fig. 4b shows the fracture azimuth population collected in the western sector of the Valle del Leone area (Fig. 4a,c). Fracture azimuth varies between N6°E and N100°E. We fitted this population with a polymodal Gaussian distribution (e.g. Salvini et al., 1999). Average values of fracture azimuth from the Gaussian fits are N64°E, N44°E and N78°E, from the most to the least frequent (Fig. 4b).

In Fig. 4d we schematically sectioned the graben of the Valle del Leone area (Fig. 4c), in which we observed a central block downthrown along two antithetic faults generated by horizontal extension. We observed these faults as high-angle ($>60°$) surfaces on the ground-surface exposure (Fig. 4c). We measured fault net throws (T1 and

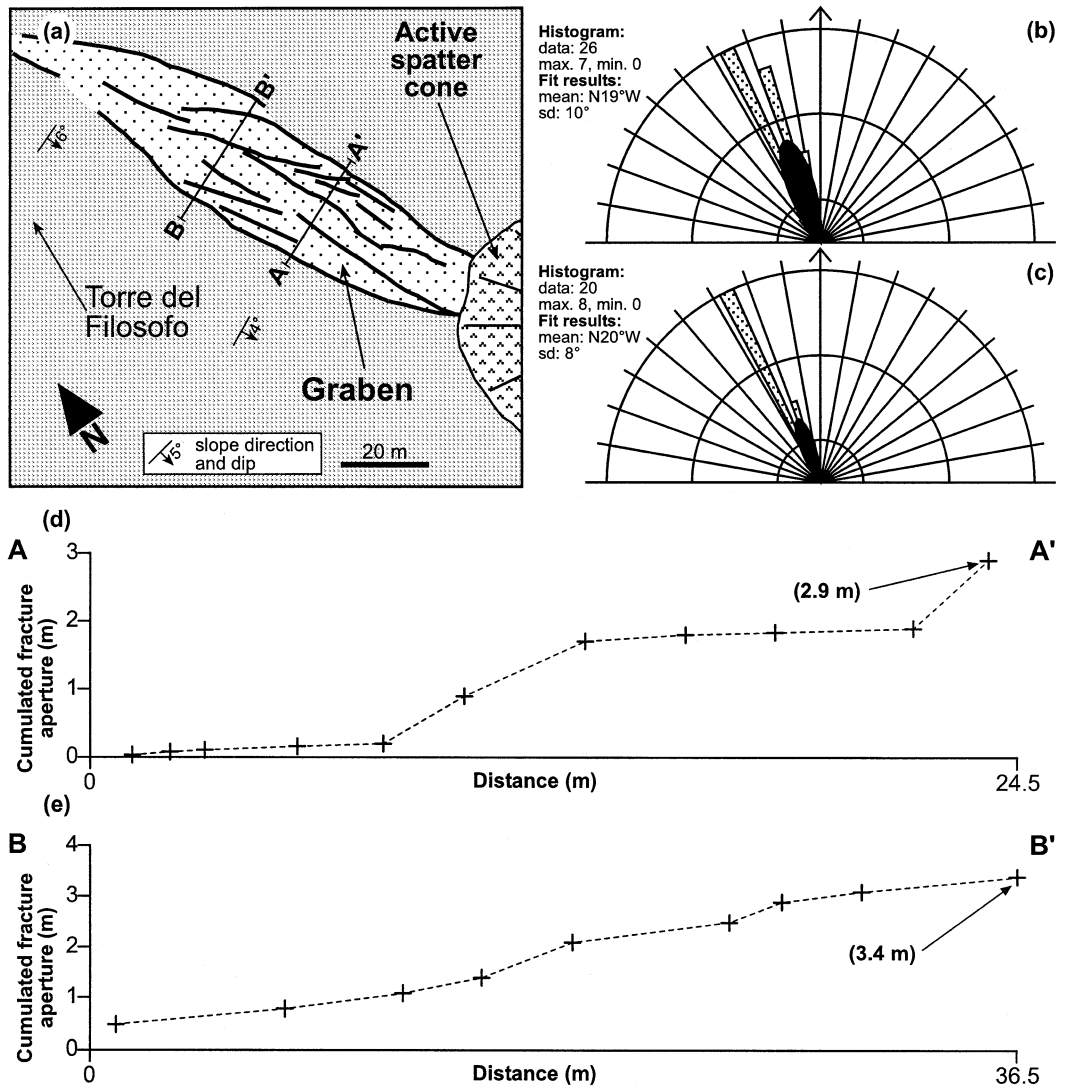


Fig. 3. (a) Structural map of the Torre del Filosofo study area. (b) Histogram (grey) and Gaussian best fit (black) of fracture azimuths collected in the Torre del Filosofo area. (c) Histogram (grey) and Gaussian best fit (black) of fracture azimuths collected along the A–A′ and B–B′ scan lines. (d) Diagram of the fracture aperture cumulated along A–A′ plotted against the A–A′ distance. (e) Diagram of the fracture aperture cumulated along B–B′ plotted against the B–B′ distance.

T2 in Fig. 4d) and heaves (H1 and H2 in Fig. 4d) in the field. The net horizontal extension (H1+H2) is about 10 m. By applying the modifications to Wallace's (1980) equations operated by Caskey (1995), the net dip slip (DS) and the master fault dip ($\theta_d$) can be computed from T1, T2, H1 and H2 according to the following equations:

$$DS = [(T1-T2)^2 + (H1+H2)^2]^{1/2} = [(5.5-3.0)^2 + (6.5+3.5)^2]^{1/2} = 10.3\ (\pm 1.3)\ \text{m} \quad (1)$$

and

$$\theta_d = \tan^{-1}[(T1-T2)/(H1+H2)] = \tan^{-1}[(5.5-3.0)/(6.5+3.5)] \approx 14^\circ\ (\pm 7^\circ) \quad (2)$$

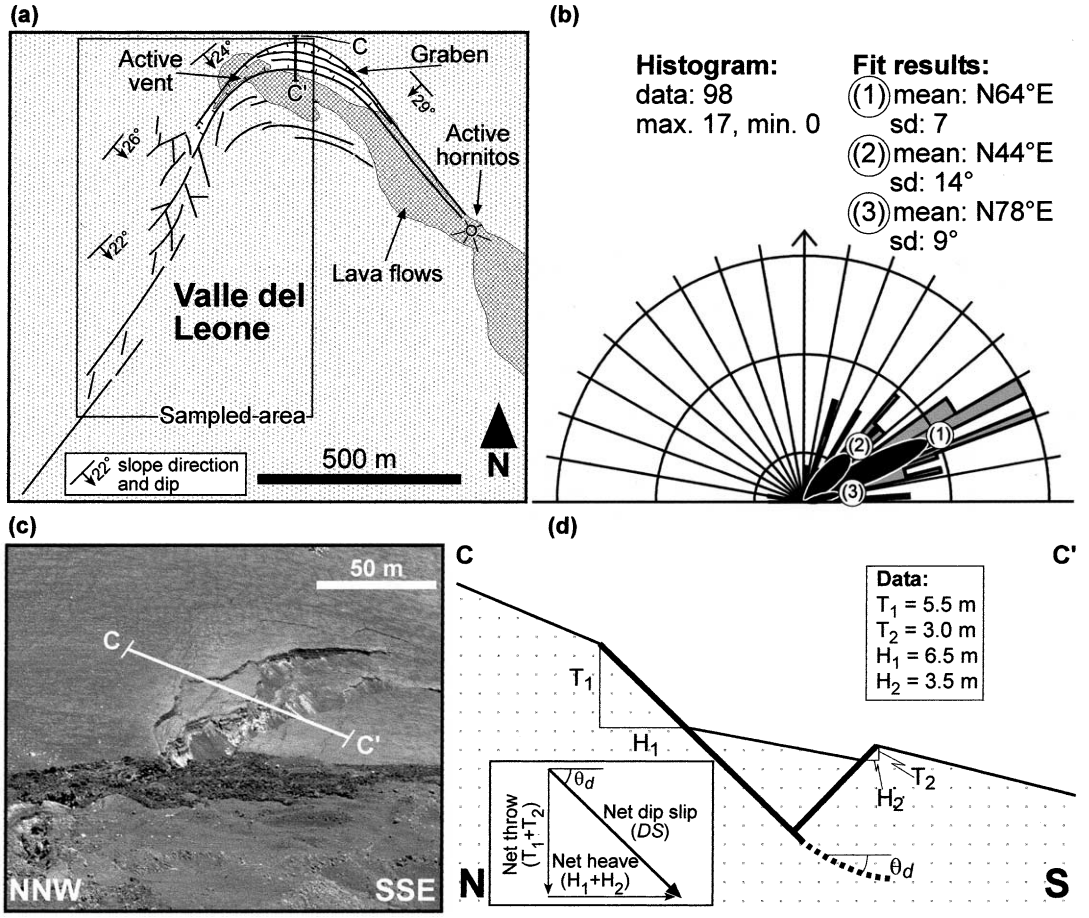


Fig. 4. (a) Structural map of the Valle del Leone study area. (b) Histogram (grey) and Gaussian best fits of fracture azimuths collected in the Valle del Leone area. (c) Photograph (21 July 2001, 14.00 h GMT) of the graben developed in the Valle del Leone area. (d) Schematic C–C′ cross-section.

The accuracy of data used in Eqs. 1 and 2 is 0.5 m. In particular, Eq. 2, from which we determine the inclination of the fault dip-slip vector (Caskey, 1995), gives an estimation of the fault dip ($\theta_d$) at the structural level beneath the graben (Fig. 4d). However, this estimation may be affected by uncertainties due to the fact that some deformation may be lost between deeper levels and the ground surface (Caskey, 1995).

From the attitude and dimensions of the graben in the Valle del Leone, we can assess a slump section surface (Fig. 4d) between 0.0015 and 0.0018 km$^2$, a slump length of at least 1 km and a volume of the involved rock mass of about $1.5\times10^{-3}$ km$^3$.

## 5. Discussion

The evidence presented above suggests a causal relationship between extensional fracturing and faulting of the ground surface and the intrusion of a system of progressively shallower feeder dykes associated with the ongoing eruption of Mt. Etna. Dyke intrusion was signalled by migration to the surface of a swarm of earthquakes (Patanè et al., 2002). The onset of the eruption and that of the ground-surface fracturing were correlated in time with the arrival of the earthquake swarm front, several hours after the initiation of dyke propagation. This indicates that the dyke intrusion triggered the ground-surface frac-

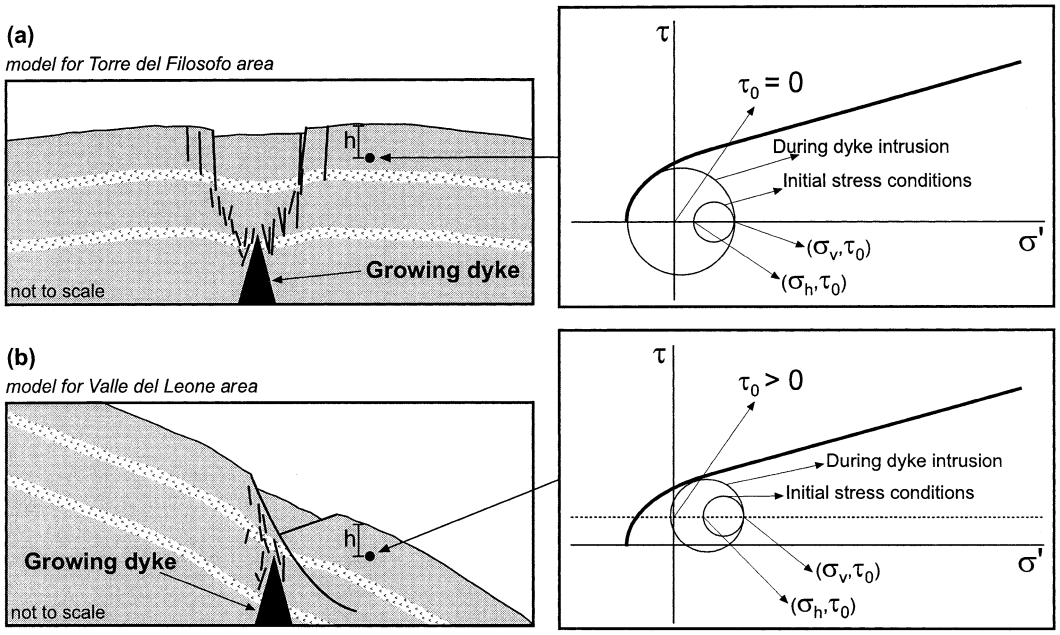


Fig. 5. Models for development of grabens (a) in the Torre del Filosofo area (modified after Mastin and Pollard, 1988) and (b) in the Valle del Leone area. Mohr diagrams are indicative of stress conditions for near-surface rocks (see arrows for indicative location). In the Valle del Leone area the initial conditions of shear stress ($\tau_0$) along the slope are represented in the Mohr diagram by a positive translation of the abscissa (dotted axis in the Mohr diagram).

turing and not vice versa (e.g. Rubin and Pollard, 1988; Bousquet and Lanzafame, 2001).

The onset and evolution of the ground-surface fracturing, together with the evolution of the eruption, suggest the following sequence of mechanisms for surface deformation above the intruding dykes. Vertical fractures and perhaps faults developed around the growing dyke top in the subsurface (Fig. 5). Extension in the subsurface produced highs and troughs on the surface (Fig. 5a). With progressing extension and upward propagation of dyke, failure reached the ground surface, and the eruption started. The following days, the fracture system propagated along the NNE–SSW direction, parallel to the Valle del Bove rim. The arc-shaped graben that formed along the steep flank at the Valle del Leone area may be interpreted as an incipient slope failure triggered by dyke emplacement. The estimated fault dip of only 14° at structural levels beneath the graben supports this interpretation. According to this model, growing extension in the subsurface produced fracturing on the surface, analogously to the Torre del Filosofo area, and triggered a slope failure where the stress regime was close to the failure conditions owing to the steep geometry of the flank (Fig. 5b). In particular, the investigated sites differ by the initial stress conditions (i.e. prior to dyke intrusion). Prior to dyke intrusion, apart from possible tectonic stresses, in the subsurface beneath the Torre del Filosofo area the vertical stress ($\sigma_v$ in Fig. 5a) was equal to the lithostatic load, the horizontal stress ($\sigma_h$ in Fig. 5a) was roughly one third the vertical stress (i.e. by considering a roughly elastic medium as suggested by the occurrence of fractures; see also Turcotte and Schubert, 1982), and the shear stress ($\tau_0$ in Fig. 5a) parallel to the surface (i.e. horizontal) was null. Dyke intrusion modified the horizontal stress and led to rock extensional failure (i.e. the Mohr circle approached the Mohr envelope in the extensional fracturing field; Fig. 5a). In the Valle del Leone area, prior to dyke intrusion, at the same depth ($h$ in Fig. 5), the vertical and horizontal stresses had the same values as in the Torre del Filosofo area, apart for the non-

zero shear stress ($\tau_0$ in Fig. 5b) parallel to the slope surface that added positive components to both the vertical and the horizontal stresses. During dyke intrusion, the Mohr circle must have rapidly approached the failure envelope in the $\tau$-$\sigma$ positive space and shear faulting occurred (e.g. Mandl, 1999). The dyke intrusion in the Valle del Leone area resulted in the development of two conjugate faults that formed a graben in which the horizontal extension (net heave in Fig. 4d) is more than three times that measured in the Torre del Filosofo area.

In the discussed model, it is necessary to distinguish surface displacements resulting from dyke opening and from fault slip (i.e. slope failure at Valle del Leone). We measured about 3 m of horizontal extension across the Torre del Filosofo graben, which lies in a flat area lateral to the Valle del Bove depression, and more than 10 m (net heave) across the Valle del Leone graben, which lies along the steep flank of the depression. The magnitude of the cumulated fracture aperture at the Torre del Filosofo area (i.e. $\sim$3 m) should be a significant fraction of the dyke width (e.g. Rubin and Pollard, 1988). On the contrary, the intrusion of a dyke perpendicular to a steep slope (i.e. Valle del Leone) was able to produce normal fault slip (i.e. slope failure) that should be greater than the dyke width (e.g. Rubin, 1992).

A comparison with fracture fields associated with past eruptions points out the significant role of fractures and slope attitude in generating fault-controlled graben subsidence and incipient slope failures. For instance, the fracture fields associated with the eruptions of Mt. Etna in 1928, 1971 and 1989, propagated from the Southeast Crater in the Valle del Leone area striking about 45° (and not parallel) to the steep slope, and formed grabens significantly narrower and shallower than that observed during the eruption of July–August 2001 (Neri et al., 1991; Ferrucci et al., 1993; Coltelli et al., 1994; Bousquet and Lanzafame, 2001).

Our results are consistent with previous works (McGuire et al., 1990, 1991; Borgia et al., 1992), which predicted the area around the Valle del Bove depression as the most probable for dyke emplacement. The N–S, 1000 m high cliff wall of the depression favours the preferential emplacement of high-level dykes parallel to the western rim, since the moving block is confined to the unbuttressed western wall (McGuire et al., 1990, 1991; Ferrari et al., 1991; Neri et al., 1991; Monaco et al., 1997; Bousquet and Lanzafame, 2001). The fracture system that developed parallel to the depression rim during the July–August 2001 Mt. Etna eruption confirms this model and highlights the role of pre-existing topography in the high-level intrusive activity (e.g. Dowden et al., 1995, 1997). The presence along the western rim of the Valle del Bove depression, of N–S, sub-vertical to downhill dipping (55° to 90°) dykes, 2 m in average thickness (Ferrari et al., 1991) suggests the above-discussed model to be a rule for Mt. Etna, at least in the area adjacent to the Valle del Bove depression. Dilation associated with magma intrusion leads in turn to periodic phases of slope instability and failure of the cliff wall, causing a progressive westward migration of the western rim (McGuire et al., 1990). The stress regime generated as a consequence of the depression's existence results in the repeated injection of N–S-oriented dykes adjacent to the western rim.

## 6. Conclusions

(1) Dyke emplacement during the July–August 2001 eruption of Mt. Etna generated different styles of deformation, as observed on the ground surface, in areas with different slope attitudes.

(1.1) Extensional fractures and associated slight graben subsidence developed in the almost flat Torre del Filosofo area, where fractures strike parallel to the gentle slope.

(1.2) Extensional fractures and faults with associated graben subsidence and incipient slope failure developed in the steep Valle del Leone area, where fractures strike perpendicular to the slope.

(2) Although voluminous flank collapses have not been recorded in recent times in the Valle del Bove area, the distribution of dykes associated with past eruptions (i.e. parallel to the slope of the Valle del Bove; Ferrari et al., 1991) suggests that failure events similar or broader than that observed at the Valle del Leone in 2001 would

have been common features along the slope of the Valle del Bove where they produced a progressively westward retreat of the depression rim by repeated slumps and collapses. However, dyke-induced slumps such as that discussed in this paper were not observed during previous eruptions at Mt. Etna, probably owing to different striking angles between dykes and the Valle del Bove slope (Ferrucci et al., 1993).

(3) Our results confirm previous models by McGuire et al. (1990, 1991) and Borgia et al. (1992), in which the rim of the Valle del Bove depression was deemed the most probable location for potential slope failure. From the attitude and dimensions of faults and associated grabens in the Valle del Leone area we can infer that such a slump (Fig. 4d) may have moved a small to intermediate rock mass (i.e. about $1.5\times10^{-3}$ km$^3$). Nonetheless, a broader shallow intrusive activity such as that testified in the past for Mt. Etna (McGuire, 1983) may produce a greater horizontal extension in the region of the Valle del Bove and subsequently a potentially large ($>0.1$ km$^3$) flank collapse.

## Acknowledgements

The authors would like to express their thanks to F. Barberi and M. Carapezza for meaningful discussions during fieldwork. F. Salvini is thanked for thoughtful comments on fracture mechanics and for kindly providing Daisy 2.0 software for structural analysis. C. Faccenna and F. Storti are thanked for encouragement and suggestions. S. Tavani is thanked for discussions on the accuracy of data and uncertainty of results. A.B. acknowledges financial support by the GNDT Geostar Project co-ordinated by L. Beranzoli at the INGV (Rome, Italy). Insightful reviews by E.A. Parfitt and an anonymous reviewer significantly improved the manuscript.

## References

Abdallah, A., Courtillot, V., Kasser, M., Le Dain, A.Y., Lepine, J.C., Robineau, B., Ruegg, J.C., Tapponier, P., Tarantola, A., 1979. Afar seismicity and volcanism to the mechanics of accreting plate boundaries. Nature 282, 17–23.

Allard, P., Carbonelle, J., Dajlevic, D., Le Bronec, J., Morel, P., Robe, M.C., Maurenas, J.M., Faivre-Pierret, R., Martin, D., Sabroux, J.C., Zettwoog, P., 1991. Eruptive and diffuse emissions of $CO_2$ from Mount Etna. Nature 351, 387–391.

Allard, P., Philippe, J.-B., D'Alessandro, W., Parello, F., Parisi, B., Flehoc, C., 1997. Mantle-derived helium and carbon in groundwaters and gases of Mount Etna, Italy. Earth Planet. Sci. Lett. 148, 501–516.

Azzaro, R., 1999. Earthquake surface faulting at Mount Etna volcano (Sicily) and implications for active tectonics. J. Geodyn. 28, 193–213.

Barberi, F., Civetta, L., Gasparini, P., Innocenti, F., Scandone, R., Villari, L., 1974. Evolution of a section of the Africa–Europe plate boundary: paleomagnetic and volcanologic evidence from Sicily. Earth Planet. Sci. Lett. 22, 123–132.

Bjornsson, A., Saemundsson, K., Einarsson, P., Tryggvason, E., Gronvald, K., 1977. Current rifting episode in north Iceland. Nature 266, 318–323.

Bonaccorso, A., 1999. The March 1981 Mount Etna eruption inferred through ground deformation modelling. Phys. Earth Planet. Inter. 112, 125–136.

Borgia, A., Ferrari, L., Pasquarè, G., 1992. Importance of gravitational spreading in the tectonic and volcanic evolution of Mount Etna. Nature 357, 231–235.

Bousquet, J.-C., Lanzafame, G., Villari, L., 1984. Les ruptures de la surface liées à l'éruption du 28 mars 1983 de l'Etna (Sicile). Bull. Volcanol. 47, 896–907.

Bousquet, J.-C., Lanzafame, G., 2001. Nouvelle interprétation des fractures des éruptiones latérales de l'Etna: conséquences pour son cadre tectonique. Bull. Soc. Géol. Fr. 172, 455–467.

Calvari, S., Groppelli, G., Pasquarè, G., 1992. Preliminary geological data on the south-western walls of Valle del Bove, Mt. Etna (Sicily). Acta Vulcanol. 5, 15–30.

Caskey, S.J., 1995. Geometric relations of dip slip to a faulted ground surface: new nomograms for estimating components of fault displacement. J. Struct. Geol. 17, 1197–1202.

Cocina, O., Neri, G., Privitera, E., Spampinato, S., 1997. Stress tensor computations in the Mount Etna area (southern Italy) and tectonic implications. J. Geodyn. 23, 109–127.

Coltelli, M., Del Carlo, P., Vezzoli, L., 1998. Discovery of a Plinian basaltic eruption of Roman age at Etna volcano, Italy. Geology 26, 1095–1098.

Coltelli, M., Garduño, V.H., Neri, M., Pasquarè, G., Pompilio, M., 1994. Geology of northern wall of Valle del Bove, Etna (Sicily). Acta Vulcanol. 5, 15–30.

Condomines, M., Tanguy, J.C., Michaud, V., 1995. Magma dynamics at Mt. Etna constraints from U-Th-Ra-Pb radioactive disequilibria and Sr isotopes in historical lavas. Earth Planet. Sci. Lett. 132, 25–41.

Day, S.J., Carracedo, J.C., Guillou, H., Gravestock, P., 1999. Recent structural evolution of the Cumbre Vieja volcano, La Palma, Canary Islands: volcanic rift zone reconfiguration as

a precursor to volcano flank instability? J. Volcanol. Geotherm. Res. 94, 135–167.
Dobran, F., Coniglio, S., 1996. Magma ascent and simulations of Etna's eruptions aimed at internal system definition. J. Geophys. Res. 101, 713–731.
Dowden, J.M., Murray, J., Kapadia, P., 1995. Mathematical modelling of the stress regime in Mount Etna using ground deformation measurements 1987–92. Tectonophysics 249, 141–154.
Dowden, J.M., Murray, J., Kapadia, P., 1997. Changes in the stress regime and displacement field in the interior of Mount Etna deduced from surface observations. Tectonophysics 269, 299–315.
Ellis, M., King, G., 1991. Structural control of flank volcanism in continental rifts. Science 254, 839–842.
Elsworth, D., Carracedo, J.C., Day, S.J. (Eds.), 1999. Deformation and flank instability of oceanic island volcanoes: a comparison of Hawaii with Atlantic Island Volcanoes. J. Volcanol. Geotherm. Res. 94 (Special Issue), 1–340.
Elsworth, D., Day, S.J., 1999. Flank collapse triggered by intrusion: the Canarian and Cape Verde Archipelagoes. J. Volcanol. Geotherm. Res. 94, 323–340.
Ferrari, L., Garduño, V.H., Neri, M., 1991. I dicchi della Valle del Bove, Etna: un metodo per stimare le dilatazioni di un apparato vulcanico. Mem. Soc. Geol. Ital. 47, 495–508.
Ferrucci, F., Rasà, R., Gaudiosi, G., Azzaro, R., Imposa, S., 1993. Mt. Etna: a model for the 1989 eruption. J. Volcanol. Geotherm. Res. 56, 35–56.
Fink, J.H., 1985. Geometry of silicic dikes beneath the Inyo domes, California. J. Geophys. Res. 90, 11127–11133.
Fink, J.H., Pollard, D.D., 1983. Structural evidence for dikes beneath silicic domes, Medicine Lake Highland Volcano, California. Geology 11, 458–461.
Finn, C.A., Sisson, T.W., Deszcz-Pan, M., 2001. Aerogeophysical measurements of collapse-prone hydrotermally altered rocks on Mount Rainier volcano. Nature 409, 600–603.
Garduño, V.H., Neri, M., Pasquarè, G., Pompilio, M., Borgia, A., Tibaldi, A., 1997. Geology of NE-rift of Mount Etna, Sicily (Italy). Acta Vulcanol. 9, 91–100.
Gillot, P.Y., Kieffer, G., Romano, R., 1994. The evolution of Mount Etna in the light of potassium-argon dating. Acta Vulcanol. 5, 81–87.
Gudmundsson, A., 1983. Form and dimensions of dykes in eastern Iceland. Tectonophysics 95, 295–307.
Gudmundsson, A., 1995. The geometry and growth of dykes. In: Baer, G., Heimann, A. (Eds.), Physics and Chemistry of Dykes. Balkema, Rotterdam, pp. 23–34.
Hoffmann, J.P., Ulrich, G.E., Garcia, M.O., 1990. Horizontal ground deformation patterns and magma storage during the Puu Oo eruption of Kilauea volcano, Hawaii: episodes 22–42. Bull. Volcanol. 52, 522–531.
Holcomb, R.T., Searle, R.C., 1991. Large landslides from oceanic volcanoes. Mar. Geotechnol. 10, 19–32.
Lanzafame, G., Leonardi, A., Neri, M., Rust, D., 1997a. Late overthrust of the Apennine-Maghrebian Chain at the NE periphery of Mt. Etna, Italy. C.R. Acad. Sci. Paris IIa 324, 325–332.
Lanzafame, G., Neri, M., Coltelli, M., Lodato, L., Rust, D., 1997b. North-south compression in the Mt. Etna region (Sicily): spatial and temporal distribution. Acta Vulcanol. 9, 121–133.
Mandl, G., 1999. Faulting in Brittle Rocks. Springer, Berlin.
Masson, D.G., Watts, A.B., Gee, M.J.R., Urgeles, R., Mitchell, N.C., Le Bas, T.P., Canals, M., 2002. Slope failures on the flanks of the western Canary Islands. Earth-Sci. Rev. 57, 1–35.
Mastin, L.G., Pollard, D.D., 1988. Surface deformation and shallow dike intrusion processes at Inyo Craters, Long Valley, California. J. Geophys. Res. 93, 13221–13235.
McGuire, W.J., 1983. Prehistoric dyke trends on Mount Etna; implications for magma transport and storage. Bull. Volcanol. 46, 9–22.
McGuire, W.J., Howarth, R.J., Firth, C.R., Solow, A.R., Pullen, A.D., Saunders, S.J., Stewart, I.S., Vita-Finzi, C., 1997. Correlation between rate of sea level change and frequency of explosive volcanism in the Mediterranean. Nature 389, 473–476.
McGuire, W.J., Pullen, A.D., Saunders, S.J., 1990. Recent dyke-induced large-scale block movement at Mount Etna and potential slope failure. Nature 343, 357–359.
McGuire, W.J., Murray, J.B., Pullen, A.D., Saunders, S.J., 1991. Ground deformation monitoring at Mt. Etna; evidence for dyke emplacement and slope instability. J. Geol. Soc. London 148, 577–583.
Mogi, K., 1958. Relations between the eruptions of various volcanoes and the deformations of the ground surfaces around them. Bull. Earthq. Res. Inst. 36, 99134.
Monaco, C., Tapponier, P., Tortorici, L., Gillot, P.Y., 1997. Late Quaternary slip rates on the Acireale-Piedimonte normal faults and tectonic origin of Mt. Etna (Sicily). Earth Planet. Sci. Lett. 147, 125–139.
Moore, J.G., Moore, G.W., 1984. Deposit from a giant wave on the island of Lanai, Hawaii. Science 226, 1312–1315.
Morgan, W.J., 1991. Surface deformation caused by a dike overlain by a layer of Coulomb material. EOS 72, 262.
Murray, J.B., Pullen, A.D., 1984. Three dimensional model of the feeder conduit of the 1983 eruption of Mt. Etna volcano, from ground deformation measurements. Bull. Volcanol. 47, 1145–1163.
Neri, M., Garduño, V.H., Pasquarè, G., Rasà, R., 1991. Studio strutturale e modello cinematico della Valle del Bove e del versante nord-orientale etneo. Acta Vulcanol. 1, 17–24.
Okamura, A.T., Dvorak, J.J., Koyanagi, R.Y., Tanigawa, W.R., 1988. Surface deformation during dike propagation. U.S. Geol. Surv. Prof. Pap. 1463, 165–181.
Parfitt, E.A., Peacock, D.C.P., 2001. Faulting in the South Flank of Kilauea Volcano, Hawaii. J. Volcanol. Geotherm. Res. 106, 265–284.
Patanè, D., Chiarabba, C., Cocina, O., De Gori, P., Moretti, M., Boschi, E., 2002. Tomographic images and 3D earthquake locations of the seismic swarm preceding the 2001 Mt. Etna eruption: evidence for a dyke intrusion. Geophys. Res. Lett. 29, 2.1–2.4.
Peacock, D.C.P., Parfitt, E.A., 2002. Active relay ramps and

normal fault propagation on Kilauea Volcano, Hawaii. J. Struct. Geol. 24, 729–742.

Pollard, D.D., Delaney, P.T., Duffield, W.A., Endo, E.T., Okamura, E.T., 1983. Surface deformation in volcanic rift zones. Tectonophysics 94, 541–584.

Reid, M.E., Sisson, T.W., Brien, D.L., 2001. Volcano collapse promoted by hydrothermal alteration and edifice shape, Mount Rainier, Washington. Geology 29, 779–782.

Romano, R., 1982. Succession of the volcanic activity in the etnean area. Mem. Soc. Geol. Ital. 23, 27–38.

Rubin, A.M., 1992. Dike-induced faulting and graben subsidence in volcanic rift zones. J. Geophys. Res. 97, 1839–1858.

Rubin, A.M., Pollard, D.D., 1988. Dike-induced faulting in rift zones of Iceland and Afar. Geology 16, 413–417.

Rymer, H., Murray, J.B., Brown, G.C., Ferrucci, F., McGuire, W.J., 1993. Mechanism of magma eruption and emplacement at Mount Etna between 1989 and 1992. Nature 361, 439–441.

Salvini, F., Billi, A., Wise, D.U., 1999. Strike-slip fault-propagation cleavage in carbonate rocks: the Mattinata Fault Zone, Southern Apennines, Italy. J. Struct. Geol. 21, 1731–1749.

Siebert, L., 1984. Large volcanic debris avalanche, characteristics of source areas, deposits and associated eruptions. J. Volcanol. Geotherm. Res. 22, 220–235.

Siebert, L., Glicken, H., Ui, T., 1987. Volcanic hazards from Bezymianny- and Bandai-type eruptions. Bull. Volcanol. 49, 435–459.

Sparks, R.S.J., Moore, J.G., Rice, C.J., 1986. The initial giant umbrella cloud of the May 18, 1980, explosive eruption of Mount St. Helens. J. Volcanol. Geotherm. Res. 28, 257–274.

Stone, R., 2001. Etna eruption puts volcano monitoring to the test. Science 293, 774–775.

Tanguy, J.C., Bucur, I., Thompson, J.F.C., 1985. Geomagnetic secular variation in Sicily and revised ages of historic lavas from Mount Etna. Nature 318, 453–455.

Turcotte, D.L., Schubert, G., 1982. Geodynamics: Applications of Continuum Physics to Geological Problems. John Wiley and Sons, New York.

van Wyk de Vries, B., Francis, P.W., 1997. Catastrophic collapse at stratovolcanoes induced by gradual volcano spreading. Nature 387, 387–390.

Voight, B., Janda, R.J., Glicken, H., Douglass, P.M., 1983. Nature and mechanics of the Mount St. Helens rockslide-avalanche of 18 May 1980. Géotechnique 33, 243–273.

Wadge, G., 1977. The storage and release of magma on Mt. Etna, Italy. J. Volcanol. Geotherm. Res. 2, 361–387.

Wallace, R.E., 1980. Discussion-nomograms for estimating components of fault displacement from measured height of fault scarp. Assoc. Eng. Geol. Bull. 17, 39–45.

Walsh, J.B., Decker, R.W., 1971. Surface deformation associated with volcanism. J. Geophys. Res. 76, 3291–3302.